https://doi.org/10.5194/hess-2020-537
Preprint. Discussion started: 27 October 2020

Hydrology and Earth System Sciences
Discussions

Machine Learning Deciphers CO_2 Sequestration and Subsurface Flowpaths from Stream Chemistry

Andrew R. Shaughnessy[1], Xin Gu[1], Tao Wen[2], Susan L. Brantley[1,2]

1. Department of Geosciences, Pennsylvania State University, University Park, PA, USA
2. Earth and Environmental Systems Institute, Pennsylvania State University, University Park, PA, USA.

Correspondence to: Andrew R. Shaughnessy (ars637@psu.edu)

Abstract. Endmember mixing analysis (EMMA) is often used by hydrogeochemists to interpret the sources of stream solutes, but variations in stream concentrations and discharges remain difficult to explain. We discovered that machine learning can be used to reveal patterns in stream chemistry that pertain to information about weathering sources of solutes and also about subsurface groundwater flowpaths. The investigation has implications, in turn, for the balance of CO_2 in the atmosphere. For example, CO_2-driven weathering of silicate minerals removes carbon from the atmosphere over ~10^6-yr timescales. Weathering of another common mineral, pyrite, releases sulfuric acid that in turn causes dissolution of carbonates. In that process, however, CO_2 is released instead of sequestered from the atmosphere. Thus, to understand long-term global CO_2 sequestration by weathering requires quantification of CO_2- versus H_2SO_4-driven reactions. Most researchers estimate such weathering fluxes from stream chemistry but interpreting the reactant minerals and acids dissolved in streams has been fraught with difficulty. We use a new machine learning technique in three watersheds to determine the minerals dissolved by each acid. The results show that the watersheds continuously or intermittently sequester CO_2 but the extent of CO_2 drawdown is diminished in areas heavily affected by acid rain. Sulfide oxidation contributes ~23% to 62% of sulfate fluxes. Without the new algorithm to deconvolve the mineral weathering, CO_2 drawdown was always overestimated. The new technique, which also elucidated the importance of different subsurface flowpaths and long-timescale changes in the watersheds, should have great utility as a new EMMA for investigating water resources worldwide.

1 Introduction

We need to understand the long-term controls on atmospheric CO_2 because of the impact of this greenhouse gas on global climate. This is important because humans are increasingly burning fossil fuels and releasing long-sequestered carbon to the atmosphere (Kasting and Walker, 1992). This new C flux upsets the natural long-term balance in the atmosphere between volcanic degassing and weathering-induced drawdown of CO_2 over millennial timescales. Chemical weathering of the most common rock-forming minerals, silicates and carbonates, removes CO_2 from the atmosphere by forming dissolved inorganic carbon that is carried in rivers to the ocean (DIC; Fig. 1). Within 10^3-10^4 yr, this DIC is precipitated as marine calcite, releasing half or all of the atmospherically derived CO_2 back to the atmosphere for silicates and carbonates, respectively (Fig. 1). Thus, over this timescale, CO_2-driven weathering (CO_2-weathering) of silicates sequesters CO_2 out of the atmosphere while CO_2-weathering of carbonates neither removes nor releases CO_2 to the atmosphere (Fig. 1). Recently, researchers have emphasized that this simple picture is made more complex because of another ubiquitous mineral, pyrite (Lerman et al., 2007). When pyrite weathers, it produces sulfuric acid that also dissolves silicates and carbonates, i.e., H_2SO_4-weathering. When DIC generated

https://doi.org/10.5194/hess-2020-537
Preprint. Discussion started: 27 October 2020


Hydrology and Earth System Sciences
Discussions

through H_2SO_4-weathering of carbonates is carried to the ocean, marine calcite precipitates and releases CO_2, increasing atmosphere concentrations (Calmels et al., 2011; Torres et al., 2014; Kölling et al., 2019). Thus, determination of the weathering contributions of silicates, carbonates, and pyrite is essential toward understanding how long-term CO_2 drawdown will occur. In this paper we describe a new and powerful technique to interpret the sources of stream solutes to understand problems such as weathering. While we show the importance of this new machine learning technique to the weathering question, we also emphasize how machine learning can teach hydrogeochemists about subsurface flow paths and other characteristics of stream systems.

The most common way hydrogeochemists interpret the fluxes of weathering are to investigate stream and river chemistry. Determining the endmembers of weathering is important because streams integrate the byproducts of weathering reactions over drainage basins, allowing assessment of regional to global understanding of fluxes – but only if minerals weathered by different acid sources can be deconvoluted (Li et al., 2008; Calmels et al., 2011; Torres et al., 2016; Winnick et al., 2017; Burke et al., 2018; Killingsworth et al., 2018). In small-scale studies in the laboratory or soil profiles, mineral reactions can be inferred, but these cannot be scaled up easily (Navarre-Sitchler and Brantley 2007). Here we show that machine learning can decipher the balance of fluxes of CO_2- versus H_2SO_4-weathering over millennial timescales as written in stream chemistry. Using a new technique, we discovered that catchments partition water into subsurface flowpaths that can be i) deciphered with respect to the extent of pyrite, silicate, and carbonate weathering in different lithologies, and ii) interpreted with respect to whether weathering is driven by CO_2 or H_2SO_4. This elucidates the long-term effects on the CO_2 balance in the atmosphere.

Although geochemists commonly use stream chemistry to determine mineral sources of solutes via weathering reactions over large aerial extents (Gaillardet et al., 1999) and hydrologists commonly use end member mixing analysis (EMMA) to determine the sources of solutes in a stream (Christophersen et al., 1990), stream datasets remain difficult to interpret because of spatial inhomogeneities and temporal variations in endmember composition. For example, sulfur isotopes in stream solutes can distinguish pyrite-derived from rain-derived sulfate because pyrite typically is depleted in ^{34}S (Burke et al., 2018; Killingsworth et al., 2018). But this attribution is difficult, more expensive, and often ambiguous because pyrite $\delta^{34}S$ varies between formations (Gautier, 1986) or within a single catchment (Bailey et al., 2004). Likewise, inputs of sulfate to watersheds, such as acid rain, can swamp out the signal from mineral reactions, and can change significantly over time (e.g., because of changing acid rain deposition) (Lynch et al., 2000; Lehmann et al., 2007). These factors make it difficult to determine sulfur sources to varying stream chemistries over time.

Several so-called “inverse models” have been used successfully to partition sulfate into endmember sources for streams and rivers. These include the two prominent modeling approaches by Torres et al. (2016) and Burke et al. (2018). However, because the chemistry of acid rain has varied over the past decades, utilizing the full range of rain chemistry in those models results in unrealistic contributions of acid rain (i.e., > 100%) or models that fail to converge. This is because the chemistry of acid rain has been so variable that it spans the entire measured range of stream samples. Additionally, utilizing the approach of Burke et al. (2018), based on the approach of Gaillardet et al. (1999), requires a priori assignment of accurate endmember chemistries. Often, the researcher must rely on a few samples to characterize endmembers, resulting in large uncertainties in endmember chemistry and in source

https://doi.org/10.5194/hess-2020-537
Preprint. Discussion started: 27 October 2020

Hydrology and Earth System Sciences
Discussions

apportioning. The machine-learning approach we describe here de-convolves sources of stream chemistry without pre-defining the endmembers. We demonstrate this with data from three well-studied watersheds with different characteristics. The new method discovers the endmember chemistries and, as a result, documents new findings of
80 importance previously undiscovered with the other methods.

In the following, we focus first on Shale Hills, an acid rain-impacted shale watershed in Pennsylvania USA with extensive data for water/rock chemistry (Jin et al., 2010; Brantley et al., 2013a; Sullivan et al., 2016). This watershed allows the most complete understanding of solute sources. Although we do not show this here, if we use either of the two previously used models for source attribution, stream chemistry data for Shale Hills either does not
85 separate acid rain and pyrite as a sulfate source (if we use the model of Torres et al., 2016) or yields a proportion for acid rain which is larger than 100% (if we use the model of Burke et al., 2018). As shown below, the NMF model easily defines endmembers and proportions.

We then show the utility of the machine learning method for watersheds where less geological information has been published: we investigate sulfide oxidation in East River and Hubbard Brook catchments. Like Shale Hills,
90 East River is shale-hosted, but it receives little acid rain (Winnick et al., 2017). In contrast, Hubbard Brook has been extensively impacted by acid rain but is underlain by schist and glacial till (Likens et al., 2002). In both cases, NMF successfully determines endmembers and source proportions.

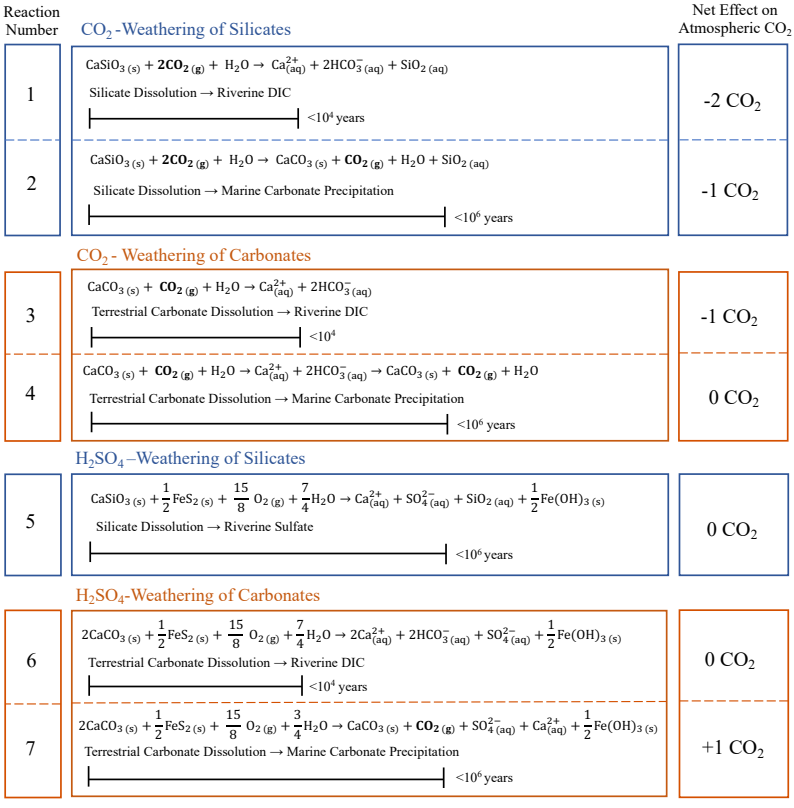

Figure 1. Schematic summarizing the reactions, timescales, and net CO_2 uptake or release for weathering of silicate and carbonate
95 **minerals at global scales by sulfuric acid and CO_2.**

https://doi.org/10.5194/hess-2020-537
Preprint. Discussion started: 27 October 2020


Hydrology and Earth System Sciences
Discussions

2 Methods

2.1 Study Sites

Where previous deconvolutions of endmembers were based on assumptions of the chemistry of dissolving minerals alone, data for watersheds shows that not only does mineral chemistry affect stream chemistry, but the flowpath of the water affects this chemistry (e.g. Brantley et al 2017). We demonstrate this with data from three well-studied watersheds with different characteristics. We focus first on Shale Hills, a small (0.08 km^2), acid-rain impacted forested watershed underlain by Rose Hill Shale located in central Pennsylvania, USA (Brantley et al., 2018). The Rose Hill Formation shale contains ~0.14 wt% S as pyrite (FeS_2) (Gu et al., 2020).

We then show utility of the method in East River (shale-hosted but it receives little acid rain) and Hubbard Brook (extensively impacted by acid rain but is underlain by schist and glacial till) catchments. Specifically, East River is a large (85 km^2), mountainous watershed underlain by Mancos Shale that is located near Gothic, Colorado USA within the Gunnison River basin (Winnick et al., 2017). The Mancos is a black shale that contains ~1.6 wt% S as pyrite (Wan et al., 2019). Lastly, Hubbard Brook (Nezat et al., 2004), located in the White Mountains of New Hampshire USA, consists of a series of nine small (0.14-0.77 km^2), forested watersheds underlain by Rangeley Formation metamorphosed shale (schist) and sandstone generally covered by glacial till derived mostly from the Kinsman granodiorite. The schist bedrock contains ~0.2-0.9 wt% S and till contains ~0.1-0.2 wt% S. Again, almost all S is present as iron sulfide (pyrite or pyrrhotite). Both bedrock and till are largely carbonate-free.

2.2 Data Acquisition

For Shale Hills, daily stream chemistry has been reported from 2008-2010 (Brantley et al., 2013b; Brantley et al., 2013c; Brantley et al., 2013d). Additional samples were measured in other time intervals for sulfur isotopes and alkalinity (Jin et al., 2014). All samples were filtered through a 0.45 μm Nylon filter and aliquots for cation analysis were acidified with nitric acid. Cations were measured on a Leeman Labs PS3000UV (Teledyne Leeman Labs, Hudson, NH) inductively coupled plasma–optical emission spectrometer (ICP-OES), and anions were measured on a Dionex Ion Chromatograph (Sunnyvale, CA). Alkalinity was measured by titration with 0.16 M H_2SO_4. Discharge data are available online (http://www.czo.psu.edu/data_time_series.html).

All published data from East River were used in analysis (Winnick et al., 2017), except for two samples with extremely high values of chloride (246 and 854 μM) because they differed significantly from the remaining sample chemistry (average Cl concentration = 21μM). Hubbard Brook weekly chemistry from 2000-2017 was downloaded for the sub-catchments (3, 6, 7, 8, 9) that were not experimentally manipulated (Bernhardt et al., 2019). Stream flow data for each sub-catchment are from USDA Forest Service (USDA, 2019).

2.3 Machine Learning Model

To assign the proportion of sulfate in streams to sources, we first bootstrapped measurements to increase data volume and then used a method of blind source separation (Alexandrov and Vesselinov, 2014; Vesselinov et al., 2018) called

https://doi.org/10.5194/hess-2020-537
Preprint. Discussion started: 27 October 2020


Hydrology and Earth System Sciences
Discussions

non-negative matrix factorization (NMF). NMF is unique from previously used methods in that it allows calculation of endmember compositions and mixing proportions simultaneously and does not rely on measurements or assumptions of endmembers a priori (Fig. 2A; see SM section 1). Specifically, NMF decomposes the *n* x *m* matrix of stream sample chemistries, *V,* into two matrices *W* and *H*:

$$V = WH \quad , \quad (1)$$

Here, *V* is an *n x m* matrix whose cell entries are solute concentration ratios, $[X]/[SO_4^{2-}]$, for stream samples. Here *n* refers to the sampling date, *m* refers to different solutes *X* (= Ca^{2+}, Mg^{2+}, Na^{+}, K^{+}, Cl^{-}), and brackets refer to concentrations. *W* is the *n* x *p* matrix whose cell entries are proportions, α, for each endmember in each stream sample. Again, *n* refers to sampling dates, but *p* is the number of sources of solutes (referred to as endmembers). The proportions refer to the fractions of sulfate in each sample that derive from an individual endmember, where the sum of proportions equals 1 ± 0.05 for each sample. As discussed later, we inferred after running the algorithm for the three watersheds that the endmembers represent different flowpaths in the subsurface. Therefore, these proportions of sulfate are referred to here as shallow, moderately shallow, and deep flowpaths, i.e. $\alpha_{shallow}$, $\alpha_{moderate}$, and α_{deep} respectively (only one of our target watersheds revealed all three flowpaths). *H* is the *p* x *m* matrix whose cell entries are the concentration ratios that define the chemical signature of each of the *p* endmembers. The key to NMF is that these concentration ratios are not determined prior to apportionment but rather are determined from the data itself. In addition, the chemical signatures of each endmember can vary temporally around central tendencies. Because the solution to eq. 1 is non-unique, we run the model 20,000 times, apply a filter to the models, and then calculate the mean and standard deviation of the remaining models for trend and error analysis (see SM section 1; Eq. S1).

The only parameter that must be defined to run NMF a priori is the number of endmembers, *p*. We used principal component analysis (PCA) to determine the number of components needed to explain >90% of the variance in stream solute ratios, and trained NMF to the bootstrapped data while assuming that number of endmembers. Machine learning determined the compositions defining the endmembers and the mixing proportions of each endmember in each sample. After running NMF, we interpreted each endmember composition based on geological and watershed knowledge.

Based on the outputs of the NMF model, we calculated the weathering rates of sulfide, carbonate, and silicate minerals in the watersheds. Additionally, we calculated the relative contributions of sulfuric and carbonic acid driving those weathering reactions. For details on the weathering calculations see SM section 2.

2.4 Synthetic Dataset

NMF is an algorithm that has been used for many applications (e.g., spectral analysis, email surveillance, cluster analysis) but not, to our knowledge, for stream chemistry (Berry et al., 2007). To exemplify the validity of our modeling approach, we generated a dataset of synthetic stream chemistry versus time and ran it through our NMF model. First, we defined known endmember compositions, which are shown in Table S4. Next we randomly generated 300 synthetic stream samples that were each calculated as a mixture of the two endmembers. Lastly, we

https://doi.org/10.5194/hess-2020-537
Preprint. Discussion started: 27 October 2020

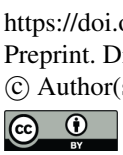

Hydrology and Earth System Sciences
Discussions
Open Access
EGU

ran NMF on the synthetic stream chemistry to determine the mixing proportions (α) and endmember compositions ($[X]/[SO_4^{2-}]$), for the five solutes.

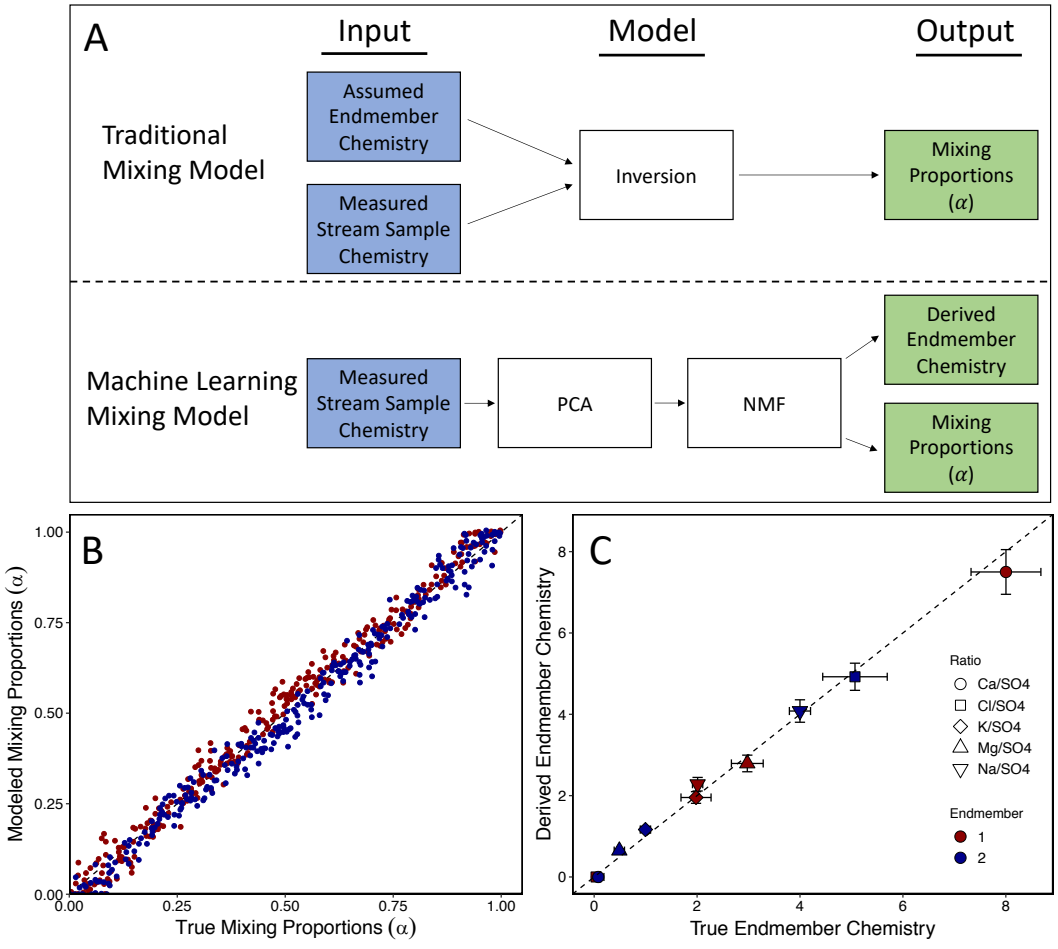

Figure 2. Schematic diagram showing the differences between input, model type, and output of a traditional mixing model and our machine learning mixing model (A). Notably, in the machine learning mixing model, endmember chemistry is not assigned *a priori*, but rather derived from patterns in the data. Results from using our machine learning mixing model (i.e., NMF) on a synthetic dataset of known endmember chemistry and mixing proportions (i.e., α) are shown in B and C. Using only the synthesized stream samples, the model adequately recovered the correct mixing proportions (B) and endmember chemistry (C).

3 Results and Discussion

3.1 Synthetic Data Model

After generating the synthetic dataset of stream samples, we utilized NMF to determine the mixing proportions and endmember compositions. We then filtered out the poor fitting models (see SM Eq. 4). As described more fully in the SM, this left an average number of valid models of 62 (range: 42-77). The average variance between valid models was <10%. Without any prior information about the system, NMF accurately determined the correct mixing

https://doi.org/10.5194/hess-2020-537
Preprint. Discussion started: 27 October 2020

Hydrology and Earth System Sciences
Discussions

proportions (RMSE = 0.04; $R^2 = 0.98$; $p < 0.001$; Fig. 2B) and endmember compositions (RMSE = 0.21; $R^2 = 0.99$; $p < 0.001$; Fig. 2C). In effect, the model was able to use patterns in the data to accurately unmix the samples.

3.2 Application to Shale Hills

While clay minerals in shale-underlain watersheds in rainy climates are found at all depths, pyrite and carbonate minerals are generally only found in unweathered shale at depth because they are depleted from upper layers (Fig. 3; Brantley et al., 2013a; Wan et al., 2019; Gu et al., 2020). For example, at Shale Hills, pyrite and carbonate minerals are only observed deeper than at least 15 meters below land surface (mbls) under the ridges and 2 mbls under the valley. In these deeper zones, calcite ($CaCO_3$), ankerite ($Ca(Fe_{0.34}Mg_{0.62}Mn_{0.04})(CO_3)_2$), and pyrite ($FeS_2$) dissolve in regional groundwaters that flow to the stream (Brantley et al., 2013a; Gu et al., 2020). These groundwaters thus contribute DIC, Ca^{2+}, Mg^{2+}, and SO_4^{2-} into the stream.

Like many catchments, water also flows to the stream in Shale Hills along a much shallower near-surface flowpath, referred to here as interflow (Fig. 3). Interflow occurs along a transiently perched water table within the upper 5-8 mbls. The most abundant mineral, illite ($K_{0.69}(Si_{3.24}Al_{0.76})(Al_{1.69}Fe^{3+}_{0.10}Fe^{2+}_{0.16}Mg_{0.19})O_{10}(OH)_2$), dissolves in interflow along a flowpath confined largely to the soil and upper weathered rock zone. Illite dissolution releases DIC and Mg^{2+} and K^+ to interflow waters and causes precipitation of clays and iron oxides. Interflow derives ultimately from local precipitation that also contains Na^+, Cl^-, and SO_4^{2-}. Interflow and deep groundwater flowlines converge under the catchment outlet where the stream, on average, is 90% interflow and 10% deep groundwater (Sullivan et al., 2016; Li et al., 2017). Only one mineral, chlorite ($(Fe^{2+}_{0.40}Mg_{0.15}Al_{0.35})_6(Si0_{.76}Al_{0.24})_4O_{10}(OH)_8$), is observed to begin to weather in the deep groundwater and continue weathering all the way to the surface (Fig. 3; Gu et al., 2020). Chlorite thus weathers to release Mg^{2+} to both interflow and deep groundwater. While most water entering the catchment leaves as interflow without entering deep groundwater, the wide reaction zone observed for chlorite is consistent with vertical infiltration of water to the deeper zone (Brantley et al., 2017).

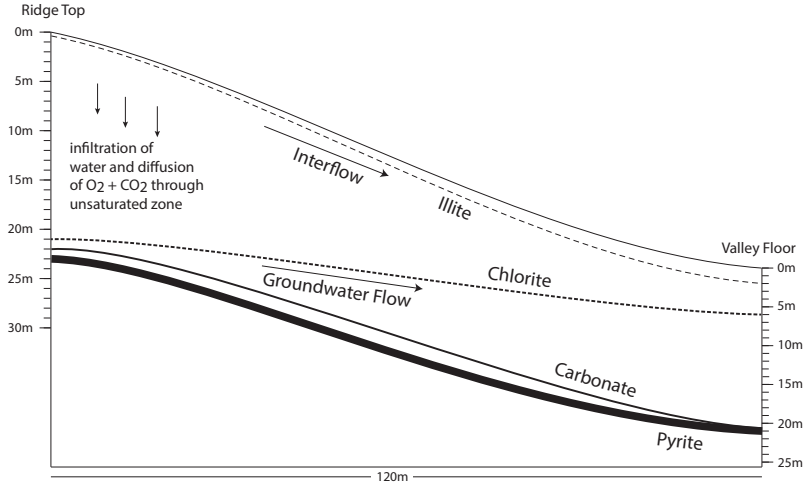

Figure 3. Schematic cross section of Shale Hills showing the depths (labelled lines) where pyrite, carbonate, chlorite, and illite reactions initiate (modified after Brantley et al., 2013a). Illite and chlorite dissolve at all depths above the labelled lines, but carbonate minerals

https://doi.org/10.5194/hess-2020-537
Preprint. Discussion started: 27 October 2020


Hydrology and Earth System Sciences
Discussions

and pyrite only dissolve in a narrow one-meter wide depth zone under the ridge that widens to tens of meters toward the valley. These reaction front depths were estimated and extrapolated from bulk chemistry measured in samples from boreholes located at the ridge and valley (Jin et al., 2010; Brantley et al., 2013a; Gu et al., 2020).

PCA for stream chemistry (2008-2010) at Shale Hills revealed two sources of sulfate, and this was used to set up NMF, i.e., $p = 2$ (Table S1). By comparing the compositions from matrix H determined by NMF to our knowledge of the subsurface (Fig. 3), we interpreted the two endmembers as deep and shallow weathering along the two flowpaths, respectively (Jin et al., 2014; Sullivan et al., 2016). The endmember with high $[Ca^{2+}]/[SO_4^{2-}]$ and $[Mg^{2+}]/[SO_4^{2-}]$ was attributed to deep weathering because Ca- and Mg-containing minerals (i.e., calcite and ankerite) only dissolve at depth (Fig. 3; Gu et al., 2020). The high $[Cl^-]/[SO_4^{2-}]$ endmember was attributed to shallow water dominated by Cl-containing rain (interflow). This attribution revealed, consistent with other studies of the acid rain-impacted northeastern United States, that precipitation accounts for the majority of sulfate flux (i.e., 77%) at Shale Hills.

Many lines of evidence back up these endmember attributions. The sulfate in the shallow endmember derives from flow well above the pyrite oxidation front through pyrite-depleted rock and is thus attributed to acid rain, while the sulfate in the deep endmember is attributed mostly to pyrite oxidation. Some sulfate from acid rain may make it to the regional groundwater, but the fraction is small. At Shale Hills, acid rain always contains Cl^- and pyrite oxidation always preferentially dissolves carbonate minerals, giving each flowpath endmember a unique signature.

To test the NMF deconvolution, we compared these attributions to isotopic data. Depletion in isotopically heavy S is observed to correlate with increasing concentrations of pyrite-derived sulfate (Fig. 4A), consistent with depleted $\delta^{34}S$ signatures in pyrite (e.g., -20‰; Killingsworth et al., 2018). In contrast, acid rain shows $\delta^{34}S$ values around +3-5‰ (Bailey et al., 2004), and low sulfate concentrations in stream samples are characterized by $\delta^{34}S$ values within this range. Also, as pyrite oxidizes, the concentration of sulfate increases and the $\delta^{34}S$ values decrease to reflect the inferred composition of pyrite, -9.5‰ to -7.2‰ (Fig. 4A). Finally, Gu et al. (2020) showed that pyrite oxidation drives the calcite dissolution at Shale Hills, and this is corroborated by NMF results showing that samples near calcite equilibrium have the highest pyrite-derived sulfate concentrations (Fig. 4B).

However, the annual flux of acid rain-derived sulfate in the shallow endmember determined from NMF at Shale Hills (Table 1) far exceeds the wet deposition of sulfate during the sampling period (Fig. 4C). But such inconsistencies have been noted elsewhere and attributed to travel-time delays over decades between acid rain input and stream output (Prechtel et al., 2001; Mörth et al., 2005). Fig. 4C thus allows us to calculate a ~19-31-year lag time between input and export of sulfate from the temporally changing acid rain input (see SM section 2.4).

Weathering profiles at Shale Hills, the chemistry of the composition (H) matrix, sulfur isotopes, calcite saturation, and lag in acid rain export all support our interpretation that the two components in the NMF model are shallow and deep flowpaths and that sulfate largely derives from acid rain and pyrite respectively.

https://doi.org/10.5194/hess-2020-537
Preprint. Discussion started: 27 October 2020

Hydrology and Earth System Sciences
Discussions

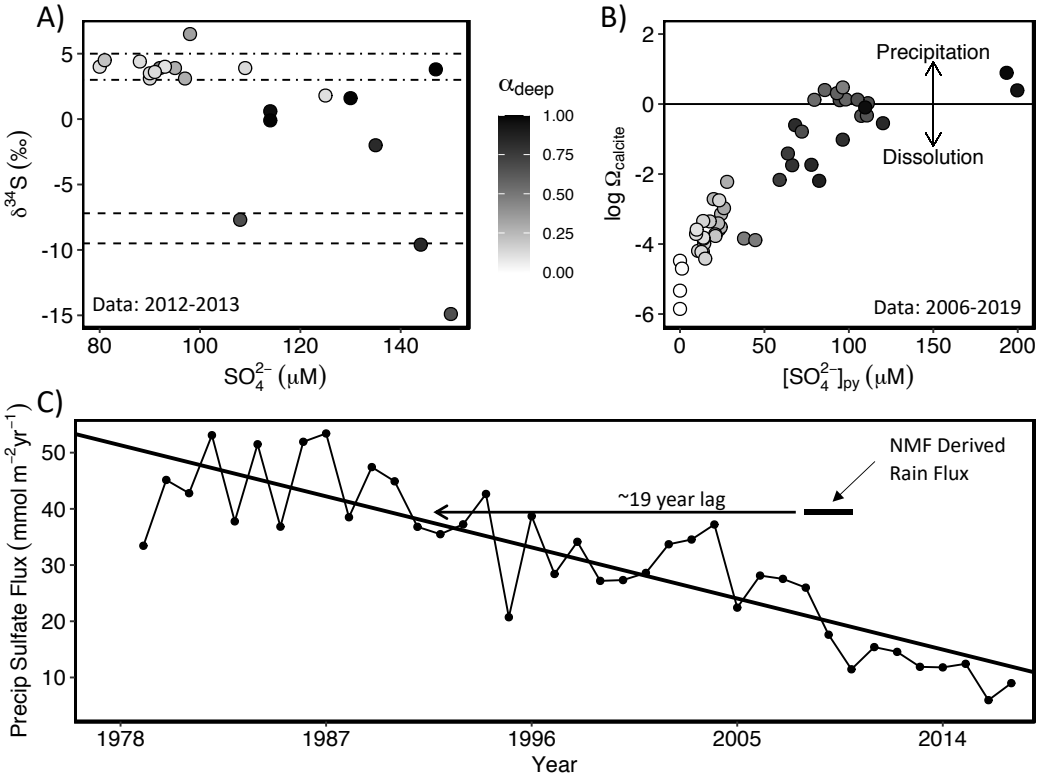

Figure 4. (A) Sulfur isotope composition plotted versus sulfate concentration in stream or groundwater at Shale Hills where S isotopes were measured (symbols; Jin et al., 2014). Dot-dashed lines represent the average sulfur isotope range for acid rain in USA (3-5‰; Bailey et al., 2004) and dashed lines represent the average sulfur isotope range of pyrite calculated from NMF results (-9.5‰ to -7.2‰). Sulfur isotopes in pyrite at Shale Hills are assumed as shown from -1‰ to -15‰ (Jin et al., 2014). (B) Plot showing the logarithm of calcite saturation index vs. the concentration of pyrite-derived sulfate (NMF-derived) in surface and groundwater at Shale Hills. Black line represents calcite solubility. Some samples in B differ from those in A because more samples were collected for alkalinity than sulfur isotopes. In both A and B, color shading represents the fraction of total sulfate derived from pyrite calculated by NMF (i.e., α_{deep}). (C) Time series plot showing the flux of sulfate in Pennsylvania NADP site PA42 (2.8 km from Shale Hills) from wet and dry deposition (see SM section 2.4). Black symbol shows the NMF results for sulfate flux derived from atmospheric inputs for Shale Hills during our sampling period, and the inferred 19 y lag.

3.3 Rates of Weathering and CO_2 Sequestration at Shale Hills

With these calculations we can use NMF results to elucidate the effect of sequestration or release of CO_2 at Shale Hills over millennial timescales. CO_2-driven weathering of the silicate minerals chlorite and illite removes carbon from the atmosphere and carries it as DIC in rivers to the ocean where it is buried as carbonate minerals (Figure 1, Table S2). In contrast, calcite and ankerite weathering coupled to pyrite oxidation instead releases CO_2 to the atmosphere over those timescales. Additionally, acid rain can interact with silicate minerals competing with CO_2 for silicate dissolution.

https://doi.org/10.5194/hess-2020-537
Preprint. Discussion started: 27 October 2020


Hydrology and Earth System Sciences
Discussions

To determine the effect on CO_2, we calculate a new parameter which we call the stream CO_2 sequestration coefficient, κ_{stream}. This coefficient, calculated for a single stream sample with units of meq CO_2/meq cation, reveals the moles of CO_2 sequestered or released during weathering per cation equivalent:

$$\kappa_{stream} = \frac{1}{2}(-1 + \gamma_{stream} + \zeta_{stream}), \quad (2)$$

Here, γ_{stream} is the proportion of cation equivalents in the stream derived from carbonate weathering, and ζ_{stream} is the proton equivalents from sulfuric acid in the stream per total base cation equivalent in the stream. We calculate γ_{stream} for a sample by multiplying the pyrite-derived sulfate concentration (i.e., α_{deep} multiplied by total sulfate concentration) by the $[Ca^{2+}]/[SO_4^{2-}]$ and $[Mg^{2+}]/[SO_4^{2-}]$ ratios of the deep weathering endmember (derived by NMF) and then dividing the result by the total concentration of base cations equivalents measured in the sample. Streams often have non-acid sources of sulfate (e.g., fertilizer, gypsum); thus, ζ_{stream} is calculated by multiplying the fraction of sulfate associated with sulfuric acid (e.g., $\alpha_{deep} + \alpha_{shallow}$) by the total sulfate concentration and dividing that by the total base cation equivalents in the sample. This calculation shows that seasonally, Shale Hills switches between net production and net consumption of CO_2 (Fig. 5D). Using the weathering reactions described in SM section 2.2, we calculate the CO_2 flux and find that annually CO_2 dynamics are net-neutral at Shale Hills (Table 1).

The switch in consumption and production is related to the dominant seasonal flowpath. In the dry season when water tables are low, the stream water is often dominated by deeper groundwater flow that interacts with the deep pyrite reaction front and has little contribution of acid rain. Even though the dry season at Shale Hills is characterized by higher contributions of pyrite-derived sulfate, the watershed acts predominantly as a sink of CO_2 during this time of the year because the drawdown of CO_2 from silicate weathering is larger than the efflux of CO_2 from pyrite-driven weathering of carbonate. In the wet season when water tables are high, the stream is dominated by shallow interflow that does not interact with pyrite but has a large contribution of acid rain. Especially during this wet season, acid rain reduces the CO_2 consumption by dissolving silicates that could otherwise have interacted with carbonic acid. This is similar to the ideas described in Kanzaki et al. (2020). The impacts of acid rain are greatest during the wet season, during which time the rain often causes the watershed to become a CO_2 source by interacting with the deep carbonate minerals and reducing the CO_2 consumption by silicate minerals.

To test the accuracy of these inferences based on NMF, we compare to previous results for Shale Hills. Based on soil pore-water chemistry and rain fluxes at Shale Hills, Jin et al. (2014) estimated the CO_2 drawdown from silicate weathering to be 44 mmol m^{-2} yr^{-1}. We find that if we assume all silicate weathering is CO_2-driven, then the silicate weathering drawdown is 38 mmol m^{-2} yr^{-1}, which is consistent with the estimate of Jin et al (2014). But this value is an overestimate that ignored pyrite and acid rain. When we correct this value for H_2SO_4-weathering of carbonate and silicate derived from pyrite and acid rain, we find that Shale Hills is actually neutral when averaged over annual timeframes and does not sequester CO_2 on net (Table 1).

https://doi.org/10.5194/hess-2020-537
Preprint. Discussion started: 27 October 2020

Hydrology and Earth System Sciences
Discussions

Table 1. Fluxes of SO_4^{2-}, Cations, and CO_2 and CO_2 Sequestration Coefficients

	Shale Hills	East River	Hubbard Brook
	Sulfate Fluxes (mmol m^{-2} yr^{-1})		
Total Sulfate	52.4 ± 5.0	198 ± 80.6	29.5 ± 0.4
Sulfide-derived Sulfate	12.1 ± 5.0	122 ± 71.8	8.6 ± 0.3
Rain-derived Sulfate	39.5 ± 6.2	76.0 ± 36.7	20.9 ± 0.4
	Fluxes (meq m^{-2} yr^{-1})[a]		
Total Cations	331 ± 78.0	1540 ± 375	76.5 ± 1.3
CO_2-weathering of Silicate Cations	29.6 ± 13.2	316 ± 252	17.5 ± 0.9
CO_2- weathering of Carbonate Cations	264 ± 59.3	588 ± 197	NA[b]
H_2SO_4- weathering of Silicate Cations	53.5 ± 10.9	152 ± 73.3	59.0 ± 0.8
H_2SO_4- weathering of Carbonate Cations	69.5 ± 23.1	489 ± 287	NA[b]
CO_2 sequestration or release	2.6 ± 6.3[c]	-35.5 ± 172	-8.7 ± 0.5
	CO_2 Sequestration Coefficients		
κ_{rock}	-0.08 ± 0.11	0.08 ± 0.17	-0.19 ± 0.11
κ_{stream}[d,e]	0.01 ± 0.03	-0.03 ± 0.11	-0.14 ± 0.06

[a]Weathering fluxes calculated following procedure in SM section 2.2
[b]No carbonate cation fluxes reported because the bedrock contains no carbonate
[c]Negative CO_2 flux indicates sequestration and positive indicates release to atmosphere
[d]Stream CO_2 sequestration coefficient reported as discharge-weighted average
[e]Rock and stream CO_2 sequestration coefficients show that Shale Hills and East River are net-neutral with respect to CO_2, and Hubbard Brook is a sink of CO_2

3.4 East River

Shale Hills is unique in that it is a monolithologic catchment and the data volume to constrain endmember apportionment is large. But NMF also works well for watersheds in which the subsurface flow and reactions are less constrained partly due to the more complex subsurface geology. The weathering profile at East River (underlain by black shale) shows that pyrite and carbonate are depleted in upper layers but start dissolving at ~2-4mbls (Wan et al., 2019). PCA shows that the number of components is 2. The composition of the endmembers for East River are similar to Shale Hills (Table S1); however, the endmember composition indicates a higher proportion of carbonate dissolution by sulfuric acid (see SM section 2).

Based on NMF for East River, pyrite contributes 62% of the annual sulfate flux (Table 1). Sulfuric acid drives 29% to 69% of carbonate dissolution depending on the season, and this compares well with previous estimates of 35-75% (Winnick et al., 2017). Unlike Shale Hills, pyrite oxidation at East River is the dominant source of sulfate because acid rain is less important, and the black shale is pyrite-rich (Fig. 5B).

Both Shale Hills and East River intermittently switch between acting as a source or sink of CO_2 (Fig. 5), and both are net neutral within error with respect to CO_2 on an annual basis. Interestingly, the seasonality of the switch between Shale Hills and East River is reversed. During baseflow (i.e., flow sustaining stream in between periods of precipitation), Shale Hills is predominantly a sink of CO_2, but sometimes it switches to a source of CO_2 in the wet season because of the impacts of acid rain. Without the large acid rain influx, East River instead acts as a sink of CO_2 during the wet season of snowmelt and then switches to a source during baseflow. This reflects that most of the

https://doi.org/10.5194/hess-2020-537
Preprint. Discussion started: 27 October 2020


Hydrology and Earth System Sciences
Discussions

sulfate at East River is derived from the pyrite-rich shale (i.e., 65%) and that H_2SO_4-weathering of carbonates is a more dominant reaction at East River than at Shale Hills. Our results are consistent with previous interpretations (Winnick et al., 2017) suggesting CO_2 efflux rates are highest in baseflow-dominated and lowest in snowmelt-dominated flow regimes. We agree with the interpretations of Winnick et al. (2017), but NMF adds the new insight that on an annual basis, the efflux of CO_2 from H_2SO_4-weathering of carbonates is balanced by CO_2-weathering of silicates making East River net neutral with respect to CO_2.

3.5. Hubbard Brook

Monolithologic shale watersheds are not the only target chemistries that can be deconvoluted with NMF. Large variations in the $\delta^{34}S$ composition of the bedrock at Hubbard Brook (Bailey et al., 2004) mean that sulfur isotopes in stream water are difficult to unambiguously apportion sulfate sources. Weathering fluxes from pyrrhotite (FeS), the sulfide mineral known to be present, have therefore never been fully constrained (Mitchell et al., 2001).

At Hubbard Brook, PCA shows three endmember sources of sulfate. As described below, we attribute these to three inferred flow lines, two in till and one at depth: waters flowing through i) shallow soil developed from till, ii) moderately-deep, less-weathered till, and iii) weathering bedrock. A three-layered weathering profile has been observed in other till-covered areas of New Hampshire as well (Goldthwait and Kruger, 1938). We used these ideas to identify endmembers as described below.

Concentrations of sulfate in acid rain have declined over time in northeastern USA (Lynch et al., 2000; Lehmann et al., 2007). Of the three NMF-determined endmembers at Hubbard Brook, two of them show declining sulfate concentrations with time. We therefore attributed the first and second endmembers to acid rain (Fig. S1).

Only one endmember showed little to no decline in sulfate concentration over time, and we therefore attributed that endmember to deep weathering in water interacting with the underlying bedrock. The composition of the deep weathering endmember shows a strong correlation between $[Mg^{2+}]/[SO_4^{2-}]$ and $[K^+]/[SO_4^{2-}]$. These compositions are similar to previous observations of weathering of metasedimentary rock piles where silicates (biotite and chlorite) are the first minerals to dissolve when sulfides oxidize (Moncur et al., 2009). Specifically, biotite ($K(Si_3Al)Mg_2FeO_{10}(OH)_2$) is known to release Mg^{2+} and K^+ while chlorite releases Mg^{2+} upon weathering. Moreover, the metamorphic conditions that produce pyrrhotite also produce biotite and chlorite, and those three minerals tend to be located together in schist foliations (Carpenter, 1974). Pyrrhotite oxidation at Hubbard Brook apparently causes dissolution of biotite $\pm$ chlorite because these are the most susceptible minerals in close proximity to the sulfide. Thus, several lines of evidence underlie our interpretation that component 3 is the deep weathering source of sulfate.

As summarized in Table 1, pyrrhotite can account for 29% of the total sulfate flux at Hubbard Brook. The schist and till contain essentially no carbonate; therefore, weathering is always a net sink for CO_2. In this watershed, however, the story is complicated by the sulfuric acid from pyrrhotite oxidation and acid rain that dissolves silicate minerals. If we had assumed all of the base cations detected in Hubbard Brook were caused by CO_2-weathering, we would have overestimated the net drawdown of CO_2 out of the atmosphere (Fig. 1). NMF deconvolutes this signal.

https://doi.org/10.5194/hess-2020-537
Preprint. Discussion started: 27 October 2020

Hydrology and Earth System Sciences
Discussions
Open Access
EGU

360

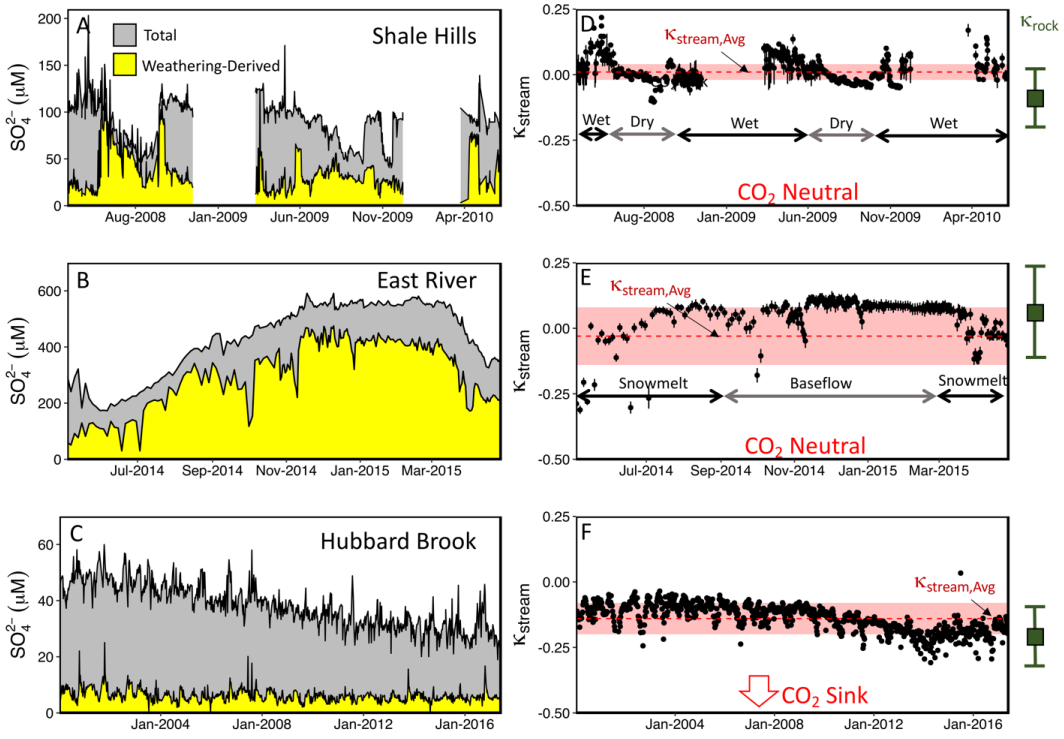

Figure 5. Concentration of total sulfate (gray) and sulfide-derived sulfate (NMF-derived; yellow) in stream water plotted versus time at Shale Hills (A), East River (B), and Hubbard Brook (W-3 sub-catchment) (C). Shale Hills and East River are net neutral, while Hubbard Brook is a net sink ($\kappa_{stream} < 0$) over the timescales studied, as shown by the CO_2 sequestration coefficient (κ_{stream}) for Shale Hills (D), East River, (E), and Hubbard Brook (F). The range (mean + 1s.d.) indicated in green to the right of D, E, and F represent κ_{rock}, the time integrated CO_2 sequestration coefficient calculated from the rock chemistry (see text). At Shale Hills and Hubbard Brook, the discharge-weighted average κ_{stream} ($\kappa_{stream,Avg}$; dashed red line) is larger than the average κ_{rock} because of acid rain, while at East River κ_{stream} is largely consistent with κ_{rock} during most of the year. The red shading on D, E, and F represents 1 s.d. from $\kappa_{stream,Avg}$. The long record at Hubbard Brook shows that κ_{stream} is approaching κ_{rock} as the watershed recovers from acid rain. Gaps in the time series for Shale Hills occur when the autosampler tubing or stream froze.

3.6 Predicting CO_2 release or drawdown from rock chemistry

From the stream chemistry, we found that Shale Hills and East River are net neutral with respect to CO_2, and Hubbard Brook is a net sink (Table 1; Figure 5). In Table 1, the weathering fluxes are simply summarized as CO_2 fluxes (see SM section 2.2), but the NMF results can also be used to calculate weathering losses for each mineral or for sulfate-driven weathering as described in SM 2.5 (Table S5). Although we do not explicitly discuss each of these additional fluxes learned from NMF, we note that the fluxes have resulted in losses of minerals from protolith as soil formed over time and we can use soil chemistry therefore as an additional test of κ_{stream}: specifically, we compare κ_{stream} to the CO_2 flux recorded in the weathered profile as solid-phase chemistry. To do this, we calculate a CO_2 sequestration coefficient analogous to κ_{stream} but instead based on rock chemistry, κ_{rock}, by assessing soil and taking

https://doi.org/10.5194/hess-2020-537
Preprint. Discussion started: 27 October 2020


Hydrology and Earth System Sciences
Discussions

into account the fraction of base cations weathered, the fraction of base cations from carbonates, and the capacity of the bedrock to produce H_2SO_4:

$$\kappa_{rock} = \frac{1}{2}(\tau + \gamma_{rock} + \zeta_{rock}), \quad (3)$$

Here, κ_{rock} is the time-integrated CO_2 sequestration coefficient determined from the solid phase weathering products in units of meq CO_2/meq base cation, τ is the mass transfer coefficient for base cations at the land surface (where 1-τ equals the fraction of cations present in original parent rock that remain in topsoil at land surface), γ_{rock} is the proportion of base cations in the bedrock associated with carbonate minerals, and ζ_{rock} is the acid generation capacity of the rock. The derivation of eq. 3 and description of each variable is more fully summarized in SM section 2.3. Briefly, γ_{rock} expresses the proportion of base cations in the parent rock that are associated with carbonate minerals (varies from 0 to 1 for 100% silicate protolith to 100% carbonate protolith). ζ_{rock} expresses the relative amount of (acid-generating) pyrite to base cations in the rock (varies from 0 to 1.5 for catchments where 100% of weathering is CO_2-driven to catchments where 100% of weathering is H_2SO_4-driven, respectively). τ expresses the fraction of cations that have not dissolved away upon exposure at the land surface (varies from -1 to 0 for 0% cations remaining at land surface to 100% cations remaining, respectively). Negative κ_{rock} is a lithology that has been net sequestering CO_2 over the duration of weathering, whereas positive κ_{rock} has been net releasing CO_2. Based on the chemistry of the bedrock and topsoil at each watershed, κ_{rock} is -0.08 ± 0.11, 0.08 ± 0.17, and -0.19± 0.11 for Shale Hills, East River, and Hubbard Brook, respectively (Tables 1, S3). Based on these values from observations of the solid weathering phases, Shale Hills and East River on net are CO_2 neutral (i.e., within error of 0), but Hubbard Brook has acted as a long-term CO_2 sink.

If the streams at each site today are acting just like the weathering recorded over the last tens of thousands of years in the solid-phase material, κ_{rock} should equal κ_{stream}. Here, we find that κ_{stream} (discharge-weighted average) for Shale Hills, East River, and Hubbard Brook are 0.01 ± 0.03, -0.03 ± 0.11, and -0.14± 0.06 respectively (Table 1). In Figure 5 we compare κ_{stream} for each sample to κ_{rock}, i.e., the time-integrated CO_2 (sequestered or released) per base cation in the parent rock. For all sites, the stream chemistry shows similar values of CO_2 sequestration coefficient for the modern (stream timescale) compared to the time-integrated (soil timescale), i.e., $\kappa_{stream} \approx \kappa_{rock}$, consistent with Shale Hills and East River acting as CO_2 net neutral but Hubbard Brook as a CO_2 sink. In addition, at Hubbard Brook, it can be seen that acid rain has competed with CO_2 in weathering minerals, lowering the capacity of the rock to sequester atmospheric CO_2, only moving back to equivalency between the rock and stream record in recent years (2013-2016; Fig. 5F) as the system recovers from acid rain.

4 Conclusions

By not requiring a priori assignments of endmembers, a new machine learning technique not only successfully reproduced source apportionments made in more traditional endmember analysis for streams, but it also revealed new information about how watersheds work. At the same time, the method also solved some issues related to source apportionment for streams with time variations of large acid rain inputs. The approach documented that two

https://doi.org/10.5194/hess-2020-537
Preprint. Discussion started: 27 October 2020


Hydrology and Earth System Sciences
Discussions

carbonate-containing shale watersheds (Shale Hills, East River) act intermittently as sources or sinks of CO_2 to the atmosphere but on net are neutral with respect to CO_2. In contrast, because it has no carbonate minerals, Hubbard Brook is a constant sink for CO_2 (Fig. 5). These observations were compared and confirmed by comparing stream chemistry to rock chemistry.

NMF also emphasized the importance of different water flowpaths in determining endmembers: the endmembers were not strictly defined by mineralogy but by patterns of subsurface flow. These flowpaths lead to patterns in stream water chemistry that were easily deciphered by our newly developed machine learning-based mixing model. In particular, for three streams, signals in the chemical variations were observed to reveal dissolution of the most reactive mineral in proximity to sulfide oxidation. Many watersheds have flowpaths distinguished by geochemical signatures from mineral reactions (Brantley et al., 2017) but we do not know these paths a priori when we investigate stream chemistry. Machine learning will be useful to model mineral reactions on broader spatial scales and will help constrain global weathering-related CO_2 dynamics because it can delineate endmembers without a priori assumptions.

Beyond these attributes, the machine learning approach also revealed other new attributes of weathering. In Shale Hills, we discovered that sulfate inputs from acid rain are not exported completely for two decades, which impacts mass balance and weathering-related CO_2 dynamics. Although not discussed explicitly here, this decadal time-lag was also observed at Hubbard Brook. NMF also showed that Hubbard Brook, recovering from the impacts of acid rain, is only recently returning to its full potential as a CO_2-sequestering rock system. In other words, prior to acid rain, Hubbard Brook sequestered more CO_2 per mole of weathered bedrock than it does today. But acid rain dissolved some of the silicates with H_2SO_4, lowering the CO_2 sequestration capability of the watershed. NMF led us to discover this new attribute of acid rain, namely that it diminishes the capacity of a rock to sequester CO_2 at millennial timescales (Figure 1) by replacement of CO_2 by H_2SO_4 as a weathering agent. Regardless of the net CO_2 dynamic, we discovered that without considering sulfide oxidation or acid rain, the CO_2 weathering sink considered over millennial timescales is always overestimated.

Acknowledgements

Financial support for this work was predominantly provided by National Science Foundation Grant EAR 13-31726 to SLB for the Susquehanna Shale Hills Critical Zone Observatory. The Shale Hills catchment is located in Penn State's Stone Valley Forest, which is funded by the Penn State College of Agriculture Sciences, Department of Ecosystem Science and Management, and managed by the staff of the Forestlands Management Office. XG acknowledges support from Office of Basic Sciences Department of Energy grant DE-FG02-05ER15675 to SLB; TW acknowledges support from Penn State College of Earth and Mineral Science Distinguished Postdoctoral Scholar Fellowship and NSF grant IIS 16-39150 to SLB; ARS acknowledges support from a Penn State University Graduate Fellowship and NSF Graduate Research Fellowship.

https://doi.org/10.5194/hess-2020-537
Preprint. Discussion started: 27 October 2020


Hydrology and Earth System Sciences
Discussions

Data Availability

Data used in analysis for this work can be found at the Susquehanna Shale Hills Critical Zone website (https://criticalzone.org/shale-hills/data), the Hubbard Brook data catalog (https://hubbardbrook.org/d/hubbard-brook-data-catalog), and in Wan et al. (2019) and in Winnick et al. (2017). Codes used in the modeling are available upon request.

Author Contributions

SLB, TW, and ARS conceived the project. TW and ARS developed the codes for the model. SLB, XG, and ARS interpreted the data and model outputs. All authors contributed in the preparation of the manuscript.

Competing Interests

The authors declare that they have no conflict of interest.

https://doi.org/10.5194/hess-2020-537
Preprint. Discussion started: 27 October 2020

References

Alexandrov, B. S., & Vesselinov, V. V. (2014). Blind source separation for groundwater pressure analysis based on nonnegative matrix factorization. *Water Resources Research*, *50*(9), 7332-7347.

Bailey, S. W., Mayer, B., & Mitchell, M. J. (2004). Evidence for influence of mineral weathering on stream water sulphate in Vermont and New Hampshire (USA). *Hydrological Processes*, *18*(9), 1639-1653.

Bernhardt E., G. Likens, E. Rosi. (2019). Continuous precipitation and stream chemistry data, Hubbard Brook Ecosystem Study, 1963 – present. Environmental Data Initiative. https://doi.org/10.6073/pasta/4022d829f3a1fa4057b63b5db8b1a172.

Berry, M. W., Browne, M., Langville, A. N., Pauca, V. P., & Plemmons, R. J. (2007). Algorithms and applications for approximate nonnegative matrix factorization. *Computational statistics & data analysis*, 52(1), 155-173.

Brantley, S. L., Holleran, M. E., Jin, L., & Bazilevskaya, E. (2013a). Probing deep weathering in the Shale Hills Critical Zone Observatory, Pennsylvania (USA): the hypothesis of nested chemical reaction fronts in the subsurface. *Earth Surface Processes and Landforms*, *38*(11), 1280-1298.

Brantley, S. L., et al. (2013b). Susquehanna Shale Hills Critical Zone Observatory Stream Water Chemistry (2008) Interdisciplinary Earth Data Alliance (IEDA). doi:10.1594/IEDA/100241

Brantley, S. L., et al. (2013c). Susquehanna Shale Hills Critical Zone Observatory Stream Water Chemistry (2009) Interdisciplinary Earth Data Alliance (IEDA). doi:10.1594/IEDA/100242

Brantley, S. L., et al. (2013d). Susquehanna Shale Hills Critical Zone Observatory Stream Water Chemistry (2010) Interdisciplinary Earth Data Alliance (IEDA). doi:10.1594/IEDA/100243

Brantley, S. L., et al. (2017). Toward a conceptual model relating chemical reaction fronts to water flow paths in hills. *Geomorphology*, *277*, 100-117.

Brantley, S. L., et al. (2018). Susquehanna Shale Hills Critical Zone Observatory: Shale Hills in the context of Shaver's Creek watershed. *Vadose Zone Journal*, *17*(1).

Burke, A., et al. (2018). Sulfur isotopes in rivers: Insights into global weathering budgets, pyrite oxidation, and the modern sulfur cycle. *Earth and Planetary Science Letters*, *496*, 168-177.

Calmels, D., Galy, A., Hovius, N., Bickle, M., West, A. J., Chen, M. C., & Chapman, H. (2011). Contribution of deep groundwater to the weathering budget in a rapidly eroding mountain belt, Taiwan. *Earth and Planetary Science Letters*, *303*(1-2), 48-58.

https://doi.org/10.5194/hess-2020-537
Preprint. Discussion started: 27 October 2020

Carpenter, R. H. (1974). Pyrrhotite isograd in southeastern Tennessee and southwestern North Carolina. *Geological Society of America Bulletin*, *85*(3), 451-456.

Christophersen, N., Neal, C., Hooper, R. P., Vogt, R. D., & Andersen, S. (1990). Modelling streamwater chemistry as a mixture of soilwater end-members. A step towards second-generation acidification models. *Journal of Hydrology*, 116(1), 307-320.

Gaillardet, J., Dupré, B., Louvat, P., & Allegre, C. J. (1999). Global silicate weathering and CO2 consumption rates deduced from the chemistry of large rivers. *Chemical geology*, *159*(1-4), 3-30.

Gautier, D. L. (1986). Cretaceous shales from the western interior of North America: Sulfur/carbon ratios and sulfur-isotope composition. *Geology*, *14*(3), 225-228.

Goldthwait, J. W., & Kruger, F. C. (1938). Weathered rock in and under the drift in New Hampshire. *Bulletin of the Geological Society of America*, *49*(8), 1183-1198.

Gu, X., et al. (2020). Chemical reactions, porosity, and microfracturing in shale during weathering: The effect of erosion rate. *Geochimica et Cosmochimica Acta*, *269*, 63-100.

Jin, L., et al. (2010). Mineral weathering and elemental transport during hillslope evolution at the Susquehanna/Shale Hills Critical Zone Observatory. *Geochimica et Cosmochimica Acta*, *74*(13), 3669-3691.

Jin, L., et al. (2014). The CO2 consumption potential during gray shale weathering: insights from the evolution of carbon isotopes in the Susquehanna Shale Hills critical zone observatory. *Geochimica et Cosmochimica Acta*, *142*, 260-280.

Kanzaki, Y., Brantley, S.L., Kump, L.R. (2020). A numerical examination of the effects of sulfide oxidation on silicate weathering. *Earth and Planetary Science Letters, 539,* 116239.

Kasting, J. F., & Walker, J. C. (1992). The geochemical carbon cycle and the uptake of fossil fuel CO2. *AIP Conference Proceedings, 247*, 175-200.

Killingsworth, B. A., Bao, H., & Kohl, I. E. (2018). Assessing pyrite-derived sulfate in the Mississippi River with four years of sulfur and triple-oxygen isotope data. *Environmental science & technology*, *52*(11), 6126-6136.

Kölling, M., et al. (2019). Consistent CO 2 release by pyrite oxidation on continental shelves prior to glacial terminations. *Nature Geoscience*, 1-6.

Lehmann, C. M., Bowersox, V. C., Larson, R. S., & Larson, S. M. (2007). Monitoring long-term trends in sulfate and ammonium in US precipitation: Results from the National Atmospheric Deposition Program/National Trends Network. In *Acid Rain-Deposition to Recovery* (pp. 59-66). Springer, Dordrecht.

https://doi.org/10.5194/hess-2020-537
Preprint. Discussion started: 27 October 2020

Lerman, A., Wu, L., & Mackenzie, F. T. (2007). CO2 and H2SO4 consumption in weathering and material transport to the ocean, and their role in the global carbon balance. *Marine Chemistry*, *106*(1-2), 326-350.

Li, S. L., Calmels, D., Han, G., Gaillardet, J., & Liu, C. Q. (2008). Sulfuric acid as an agent of carbonate weathering constrained by δ13CDIC: Examples from Southwest China. *Earth and Planetary Science Letters*, *270*(3-4), 189-199.

Li, L., et al. (2017). Understanding watershed hydrogeochemistry: 2. Synchronized hydrological and geochemical processes drive stream chemostatic behavior. *Water Resources Research*, *53*(3), 2346-2367.

Likens, G. E., et al. (2002). The biogeochemistry of sulfur at Hubbard Brook. *Biogeochemistry*, *60*(3), 235-316.

Lynch, J. A., Bowersox, V. C., & Grimm, J. W. (2000). Acid rain reduced in eastern United States. *Environmental science & technology*, *34*(6), 940-949.

Mitchell, M. J., et al. (2001). Use of stable isotope ratios for evaluating sulfur sources and losses at the Hubbard Brook Experimental Forest. *Water, Air, and Soil Pollution*, *130*(1-4), 75-86.

Moncur, M. C., Jambor, J. L., Ptacek, C. J., & Blowes, D. W. (2009). Mine drainage from the weathering of sulfide minerals and magnetite. *Applied Geochemistry*, *24*(12), 2362-2373.

Mörth, C. M., et al. (2005). Mineralization of organic sulfur delays recovery from anthropogenic acidification. *Environmental science & technology*, *39*(14), 5234-5240.

Navarre-Sitchler, A., & Brantley, S. (2007). Basalt weathering across scales. *Earth and Planetary Science Letters*, 261(1-2), 321-334.

Nezat, C. A., Blum, J. D., Klaue, A., Johnson, C. E., & Siccama, T. G. (2004). Influence of landscape position and vegetation on long-term weathering rates at the Hubbard Brook Experimental Forest, New Hampshire, USA. *Geochimica et Cosmochimica Acta*, *68*(14), 3065-3078.

Prechtel, A., et al. (2001). Response of sulphur dynamics in European catchments to decreasing sulphate deposition. *Hydrology and Earth System Sciences Discussions*, *5*(3), 311-326.

Sullivan, P. L., et al. (2016). Oxidative dissolution under the channel leads geomorphological evolution at the Shale Hills catchment. *American Journal of Science*, *316*(10), 981-1026.

Torres, M. A., West, A. J., & Li, G. (2014). Sulphide oxidation and carbonate dissolution as a source of CO2 over geological timescales. *Nature*, *507*(7492), 346.

https://doi.org/10.5194/hess-2020-537
Preprint. Discussion started: 27 October 2020


Hydrology and Earth System Sciences
Discussions

Torres, M.A., et al., 2016. The acid and alkalinity budgets of weathering in the Andes–Amazon system: Insights into the erosional control of global biogeochemical cycles. *Earth and Planetary Science Letters*, *450*, pp.381-391.

Vesselinov, V. V., Alexandrov, B. S., & O'Malley, D. (2018). Contaminant source identification using semi-supervised machine learning. *Journal of contaminant hydrology*, *212*, 134-142.

USDA Forest Service, Northern Research Station (2019). Hubbard Brook Experimental Forest: Instantaneous Streamflow by Watershed, 1956 – present. Environmental Data Initiative. https://doi.org/10.6073/pasta/282953c2290b1f00d9326ffd9a7e9668.

Wan, J., et al. (2019). Predicting sedimentary bedrock subsurface weathering fronts and weathering rates. *Scientific reports*, *9*(1), 1-10.

Winnick, M. J., et al. (2017). Snowmelt controls on concentration-discharge relationships and the balance of oxidative and acid-base weathering fluxes in an alpine catchment, East River, Colorado. *Water Resources Research*, *53*(3), 2507-2523.